Computational simulation of manufacturing processes

Towards void formation and permeability predictions in LCM processes: A computational bifluid–solid mechanics framework dealing with capillarity and wetting issues

Vers des prédictions de perméabilité et de formation de vides dans les procédés d'élaboration des matériaux composites par infusion : un modèle de contact bifluide–solide impliquant les effets de tension de surface et de mouillage

Yujie Liu, Nicolas Moulin [*], Julien Bruchon, Pierre-Jacques Liotier, Sylvain Drapier

LGF UMR CNRS 5307, École des mines de Saint-Étienne, 158, cours Fauriel, CS 62362, 42023 Saint-Étienne cedex 2, France

A B S T R A C T

A bifluid–solid contact model involving surface tension and wetting effects is developed within a finite element framework, in order to provide an accurate characterization of the fluids and fibrous behaviours during Liquid Composite Molding processes. This model is based on a Eulerian approach of two immiscible fluid (resin/air) domains with boundary conditions which prescribe wetting phenomena at fluid/fiber interfaces. The fluid interface is described by the Level Set method, on which capillary force is considered. Numerical simulations of a drop evolution with wetting effects are used to illustrate this challenging physical problem.

R É S U M É

Un modèle de contact bifluide–solide, impliquant les effets de tension de surface et de mouillage, a été développé dans un code éléments finis, afin de fournir une caractérisation précise des fluides (résine/air) et des fibres imperméables à l'échelle microscopique au cours des procédés d'élaboration des matériaux composites par infusion de résine. Ce modèle est basé sur une description eulérienne des deux fluides non miscibles et sur des conditions aux limites qui décrivent les phénomènes de mouillage aux interfaces fluides/fibres. Le front fluide est décrit par une méthode *Level set*, sur laquelle les forces

* Corresponding author.
E-mail addresses: yujie.liu@emse.fr (Y. Liu), nicolas.moulin@emse.fr (N. Moulin), bruchon@emse.fr (J. Bruchon), liotier@emse.fr (P.-J. Liotier), drapier@emse.fr (S. Drapier).

capillaires sont considérées. Les évolutions des gouttes sous l'effet du mouillage ont été simulées pour illustrer ce problème complexe.

1. Introduction

Dynamic wetting flows play an important role in various domains of engineering applications, such as petroleum, microfluidic device, lubrication and polymer processing. It involves two immiscible fluids separated by a moving interface. The dynamics of the interfaces is largely influenced by capillary forces, and the interaction of these fluids with a solid surface gives rise to wetting phenomena. This paper describes the first steps required to investigate numerically the capillary and wetting phenomena that can be met in Liquid Composite Molding processes (LCM), in order to predict voids formation and to allow a better measurement of permeabilities.

Developed in recent years, LCM processes are particularly interesting for the manufacture of large or complex composite parts. These processes consist in infusing a liquid resin into a stacking of fibrous preforms, on which a mechanical pressure field is applied. The simulation of LCM processes may involve multiple physical phenomena: fluid mechanics, solid mechanics, thermal and resin cross-linking [1]. Moreover, even if one considers only the fluid–solid mechanics, these phenomena can be described at various scales (Fig. 1): the microscopic one, which describes the flow of resin between the fibers, the mesoscopic one, where the flow of resin between the tows can be simulated, and the macroscopic scale, which corresponds to the scale of the piece.

A finite element framework based on coupling of flows in a purely fluid region, ruled by Stokes' equations, and in a porous region governed by Darcy's equations has been proposed recently, and successfully investigated for 3D industrial applications [2–4]. However, the multi-scale nature of the porous media is not included in these works, which makes it difficult to predict some phenomena such as the micro/macro-void (Fig. 2) creation, which can significantly affect the quality of composite parts. Indeed, this porosity creation is mainly due to the inhomogeneous micro-structure of the preform. The aim of the present work is to provide an accurate characterization of phenomena at the microscopic scale within a finite element framework. It involves modelling the two-phase capillary flows (air/resin) and the wetting effect between the fluids and the fibrous solid, which are determinant for the creation of micro/macro-voids and their subsequent evolution (Fig. 3).

In the past decades, various CFD techniques have been developed for modelling two-phase flows with moving interfaces. They can be either Eulerian, Lagrangian or more generally Arbitrary Lagrangian–Eulerian (ALE) methods, combined with interface capturing techniques such as the front tracking methods (maker and cell (MAC), [5]) or the front capturing methods (Level Set [6,7], Volume of fluid [8] and Phase-field method [9,10]). Every approach has its advantages and drawbacks, more descriptions of the existing various methods can be found in the literature [11,12]. As for the LCM applications, we choose the Eulerian description for the fluid domain, and the Level Set method for the interface description allowing accurate description of curved interfaces with strong topological evolutions.

However, the accurate simulation of capillary driven flows, using the finite element method, remains a challenge. It is well known that the capillary-driven flow simulation is especially difficult mainly due to the singular surface tension force, and the associated discontinuities of pressure and viscosity, etc. Moreover, spurious velocities can be observed in the vicinity of the interface when considering a standard finite element approximation in Eulerian approach, which may significantly affect precision and robustness of numerical simulations. Most recent researches focus on the improvement of existing methods [13–16]. In the present work, a robust Eulerian finite element method is proposed for the simulation of both capillary-driven flow and wetting phenomena observed in the LCM processes simulation. A Surface Local Reconstruction (SLR) method [17], which consists in reconstructing locally the fluid interface is developed for the surface tension computation, and compared with the Continuum Surface Force (CSF) method [18]. An alternative tensorial method [19,17] has also been implemented to avoid the explicit computation of the curvature (second derivative of Level Set function), which is tricky when the Level Set function is approximated with piecewise linear functions.

The physics of the wetting phenomenon is a very vast and active field of research. It has been studied by various researchers, such as in earlier studies of [20,21], and in the works of [22–26] for the computational aspects. However, the phenomenon remains partially understood and only very recent work [27–29] try to simulate capillarity using the finite element method, some of which [28,29] are based on ALE methods. Before including rather complex dynamic wetting model, only numerical methods that allow us to take into account contact angle and contact line movements are considered in the present work.

The outline of this article is as follows. In Section 2, the governing equations of fluids and moving interfaces are briefly described. In Section 3, stabilized finite element methods for the bifluid Stokes equations are recapitulated. Special attention is paid on the surface tension term computation and on taking into account the contact angle. Finally, numerical verifications and validations are presented in Section 4. An droplet in equilibrium with wall adhesion effects test case is simulated. Concluding remarks and future research perspectives are discussed in Section 5.
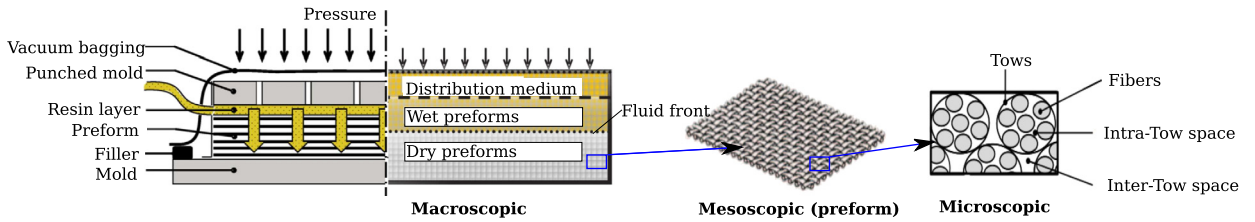
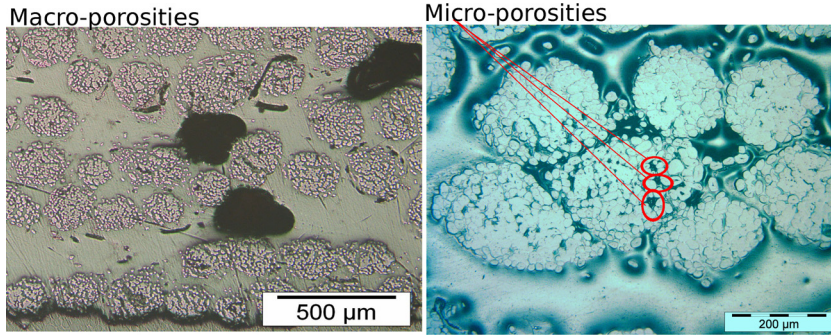**Fig. 1.** The different modelling scales of (LCM) resin-infusion-based processes.
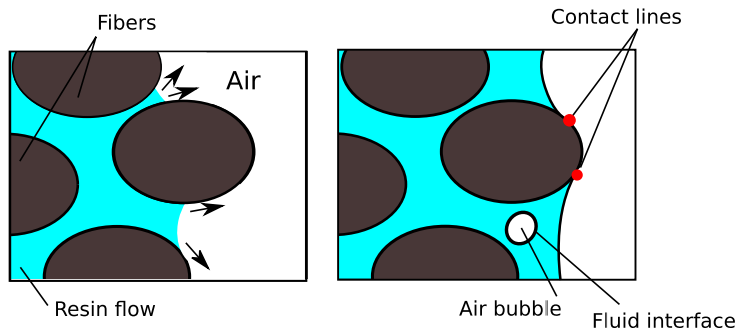

Fig. 2. Macro/micro-porosities [30].

Fig. 3. Description of the moving interfaces at the microscopic scale.

2. Governing equations

Consider here a fluid domain $\Omega \subset \mathbb{R}^d$ ($d = 2$ or $d = 3$) occupied by two immiscible incompressible Newtonian fluids: air and resin, denoted by Ω_1 and Ω_2 respectively. Its outer boundary $\partial\Omega$ can be divided into several parts, where both Neumann ($\partial\Omega_N$) and Dirichlet ($\partial\Omega_D$) boundary conditions can be applied, respectively. A set of impervious fibers Ω_S, assumed to be non-deformable, is embedded into a surrounding fluid. In this article, only the outer boundary of fibers $\partial\Omega_S$ is considered so as to take into account wetting phenomena. The domain of fibers is only represented by boundaries for simplicity. The moving interface between the two fluids, denoted by Γ, can be either closed or interact with the fluid/fibers interface $\partial\Omega_S$ (Fig. 4). In the latter case, Γ has a boundary $\partial\Gamma$, which is the so called contact point (blue dots in Fig. 4) in 2D case. θ is the associated contact angle.

2.1. Two-phase Stokes equations

Assuming that the modelling scale is small enough so that the inertial effects can be neglected. The flow of both fluids is described by one single Stokes system, expressing momentum conservation and incompressibility condition. Each fluid is distinguished by using a Heaviside function. The surface tension force is considered at the fluid interface Γ and the contact line problems are considered as boundary conditions and presented thereafter. Moreover, the volume force of gravity is also included. The Stokes equations are then expressed as: find the velocity ($\mathbf{v}$) and the pressure (p) fields defined on Ω such as:
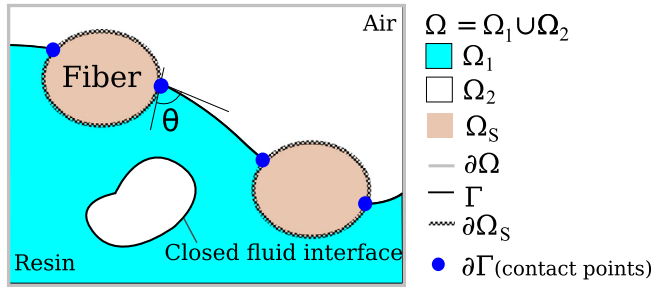
Fig. 4. 2D geometrical setting.

$$\begin{cases} -\nabla \cdot (2\eta\dot{\varepsilon}(\mathbf{v})) + \nabla p = \gamma\kappa\mathbf{n}\delta(\Gamma) + \rho\mathbf{g} & \text{in } \Omega \\ \nabla \cdot \mathbf{v} = \mathbf{0} & \text{in } \Omega \\ \mathbf{v} = \mathbf{v}_b & \text{on } \partial\Omega_D \\ \sigma_N = -p_e\mathbf{n}_b & \text{on } \partial\Omega_N \end{cases} \tag{1}$$

where η is the dynamic viscosity, $\dot{\varepsilon}(\mathbf{v}) = (\nabla\mathbf{v} + {}^t\nabla\mathbf{v})/2$ is the strain rate tensor, ρ is the density, $\mathbf{g}$ is the gravity. The surface tension force $F_\Gamma = \gamma\kappa\mathbf{n}\delta(\Gamma)$ acts only at the interface Γ. $\delta(\Gamma)$ is the Dirac function defined on the interface only, γ is the surface tension coefficient, κ the curvature of the interface and $\mathbf{n}$ its normal vector. $\mathbf{v}_b$ is the velocity prescribed on $\partial\Omega_D$. σ_N is the normal stress prescribed on boundary $\partial\Omega_N$ equal to $-p_e\mathbf{n}_b$, where p_e is a pressure to be prescribed on $\partial\Omega_N$, $\mathbf{n}_b$ is the unit vector normal to $\partial\Omega_N$. Introducing the signed distance function φ defined as:

$$\varphi(\mathbf{x}) \begin{cases} = -d(\mathbf{x}, \Gamma) \text{ if } \mathbf{x} \in \Omega_1 \\ = \;\;\, d(\mathbf{x}, \Gamma) \text{ if } \mathbf{x} \in \Omega_2 \end{cases} \tag{2}$$

where $d(\mathbf{x}, \Gamma)$ is the distance from any point $\mathbf{x}$ to the interface Γ, so Γ can be described by the iso-value of φ: $\Gamma = \{x|\varphi(\mathbf{x}) = 0\}$. The viscosity η and density ρ can be defined in terms of $\rho_i, \eta_i, i = 1, 2$ (the viscosity and the density of each fluid) using the Heaviside functions H_1 and H_2:

$$\eta = H_1(\varphi)\eta_1 + H_2(\varphi)\eta_2 \tag{3}$$

$$\rho = H_1(\varphi)\rho_1 + H_2(\varphi)\rho_2 \tag{4}$$

with:

$$H_1(\varphi) = \begin{cases} 1, \text{ if } \varphi \geq 0 \\ 0, \text{ if } \varphi < 0 \end{cases}$$

$$H_2 = 1 - H_1 \tag{5}$$

2.2. Level Set equations

The moving interface is described by the Level Set method [6,7], consisting in convecting the signed distance function φ (Eq. (2)) with the flow velocity $\mathbf{v}$:

$$\begin{cases} \dfrac{\partial\varphi}{\partial t} + \mathbf{v} \cdot \nabla\varphi = 0, & \forall(t, \mathbf{x}) \in \mathbb{R}^+ \times \Omega \\ \varphi(x, t = 0) = \varphi_0(x) & \forall x \in \Omega \\ \varphi(x, t) = g(x, t) & \forall x \in \partial\Omega^-, \forall t \in \mathbb{R}^+ \end{cases} \tag{6}$$

This equation sets the value of the Level Set function φ over the inflow boundary $\partial\Omega^-$ to be equal to $g(x, t)$. The inflow boundary is defined as: $\partial\Omega^- = \{x \in \partial\Omega|\mathbf{v} \cdot \mathbf{n} < 0\}$. One advantage of the Level Set method is that the normal vector ($\mathbf{n}$) and curvature (κ) of interface can be easily calculated:

$$\mathbf{n} = \frac{\nabla\varphi}{||\nabla\varphi||}, \; \kappa = \nabla \cdot \mathbf{n} \tag{7}$$

These geometric quantities are involved in the calculation of the surface tension term calculation, which will be detailed in section 3.2. Furthermore, since Eq. (6) does not preserve the distance function property ($||\nabla\varphi|| = 1$), an additional step, the so-called reinitialization step [31], is also considered in order to recover the unit gradient property. From a numerical point of view and in a finite element frame work, the Level Set function φ is approximated by a continuous piecewise linear function. The transport equation is then solved by using a stabilization technique SUPG (Streamline-Upwind/Petrov–Galerkin [32]).
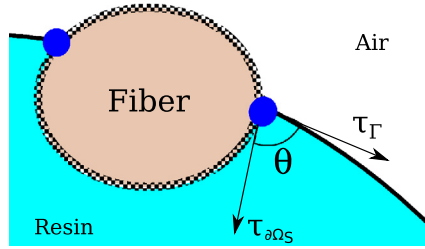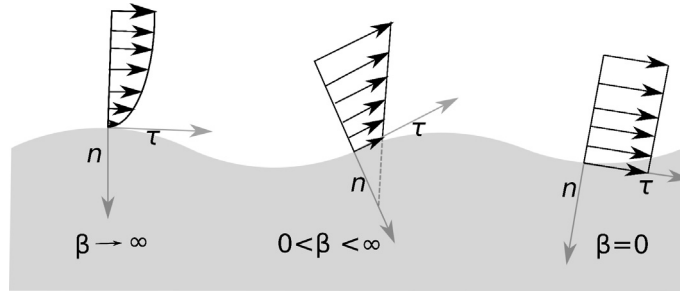
Fig. 5. Geometrical definition at contact line.

Fig. 6. Representation of the Navier boundary condition for different values of the slip coefficient β.

2.3. Boundary conditions for wetting phenomena

The contact line is line of intersection between two fluids and a fiber surface $\partial\Omega_S$, it is represented by the two blue dots in the 2D situation (Fig. 5). The boundary conditions for wetting phenomena allow us to take into account contact line dynamic. It consists in the description of the contact angle and the slip of the contact line on the fiber surface. In this work, we used an iterative method to take into account the contact angle at the fluid/fiber interfaces $\partial\Omega_S$. This method will be detailed directly in the numerical method section.

A major challenge in the simulation of the contact line dynamic is that the classical hydrodynamic equations, such as the Stokes equations, coupled with the conventional no-slip boundary condition, leads to a stress singularity at the contact line [20,25]. Various methods have been proposed recently to remove the stress singularity, such as the diffuse interface method or methods replacing the no-slip boundary condition by some slip model in the vicinity of the contact line. The Navier condition used in this work is maybe the most documented method for moving contact line simulation [33,34,22,35]. It consists of imposing a tangential force (σ_τ) at $\partial\Omega_S$ proportional to the velocity ($\mathbf{v}_\tau$) at the interface, that is:

$$\sigma_\tau \cdot \mathbf{n}_{\partial\Omega_S} = -\beta\mathbf{v}_\tau \tag{8}$$

where $\beta = 1/\lambda$ is the slip coefficient, λ is the so called slip length, which is usually estimated to be the nanometre scale. Thus, β is in general very large except in the vicinity of the contact point $\partial\Gamma$. However, a constant value of β is considered for simplicity. Flow states for different value of β are sketched in Fig. 6.

2.4. Variational formulation

Introducing the following spaces for a bounded fluid domain $\Omega \subset \mathbb{R}^d$:

$$Q(\Omega) = L^2(\Omega) = \left\{ q : \Omega \to \mathbb{R} \mid \int_\Omega q^2 \mathrm{d}\Omega < +\infty \right\}$$

$$W(\Omega) = (H^1(\Omega))^d = \left\{ \mathbf{w} \in L^2(\Omega)^d \mid \nabla\mathbf{w} \in L^2(\Omega)^{d\times d} \right\}$$

$$W_0(\Omega) = \left\{ \mathbf{w} \in H^1(\Omega)^d \mid \mathbf{w}_{|\partial\Omega_D} = 0 \right\}$$

$$W_D(\Omega) = \left\{ \mathbf{w} \in H^1(\Omega)^d \mid \mathbf{w}_{|\partial\Omega_D} = \mathbf{v}_b \right\}$$

the variational formulation of the Stokes problem reads: find $(\mathbf{v}, p) \in W_D \times Q$ such that

$$\begin{cases} \displaystyle\int_{\Omega} 2\eta\dot{\varepsilon}(\mathbf{v}) : \dot{\varepsilon}(\mathbf{w})\, \mathrm{d}V - \int_{\Omega} p\, \nabla \cdot \mathbf{w}\, \mathrm{d}V \\[2ex] = \displaystyle\int_{\Omega} \rho\mathbf{g} \cdot \mathbf{w}\, \mathrm{d}V + \int_{\Gamma} \gamma\kappa\mathbf{n} \cdot \mathbf{w}\, \mathrm{d}S + \int_{\partial\Omega_{\mathrm{N}}} (-p_{\mathrm{e}}\mathbf{n}_{\mathrm{b}}) \cdot \mathbf{w}\, \mathrm{d}S \\[2ex] + \displaystyle\int_{\partial\Omega_{\mathrm{S}}} \alpha[(\mathbf{v}\cdot\mathbf{n})]\mathbf{n} \cdot \mathbf{w}\, \mathrm{d}S - \int_{\partial\Omega_{\mathrm{S}}} \beta(\mathbf{v} - [(\mathbf{v}\cdot\mathbf{n})]\mathbf{n}) \cdot \mathbf{w}\, \mathrm{d}S \\[2ex] \displaystyle\int_{\Omega} q\, \nabla \cdot \mathbf{v}\, \mathrm{d}V = 0 \end{cases} \tag{9}$$

for all $(\mathbf{w}, q) \in W_0 \times Q$. Let us note that, the penalty method is used to ensure that the velocity in the normal direction is null on the fiber boundaries, α is the penalty parameter.

3. Numerical strategy

The Stokes equations are approximated by mixed velocity–pressure finite elements with continuous piecewise linear functions. This mixed velocity–pressure formulation is stabilized by a Variational Multi-Scale method (VMS): Algebraic Sub-Grid Scale (ASGS) defined on one single mesh. In this section, the Stokes ASGS stabilization formulation is briefly recalled. A special attention will be paid to the surface tension term and the static angle computation.

3.1. ASGS stabilization formulation for the Stokes problem

Since it is well known that the P1/P1 approximation for the Stokes' problem does not satisfy the Ladyzhenskaya–Babuška–Brezzi (LBB) condition, an ASGS (Algebraic Sub-Grid Scale) method is used to stabilize the formulation. More details can be found for this method in [36,37] for the Stokes/Darcy stabilization. Let $(W_{\mathrm{D}})_h \subset W_{\mathrm{D}}$, $Q_h \subset Q$ be the standard P1-element space for velocity and pressure, the stabilized discrete variational formulation of (9) reads: Find $(\mathbf{v}_h, p_h) \in (W_{\mathrm{D}})_h \times Q_h$ such that:

$$\begin{cases} \displaystyle\int_{\Omega} 2\eta\dot{\varepsilon}(\mathbf{v_h}) : \dot{\varepsilon}(\mathbf{w_h})\, \mathrm{d}V - \int_{\Omega} p_h\, \nabla \cdot \mathbf{w}_h\, \mathrm{d}V \\[2ex] = \displaystyle\int_{\Omega} \rho\mathbf{g} \cdot \mathbf{w}_h\, \mathrm{d}V + \int_{\Gamma} \gamma\kappa\mathbf{n} \cdot \mathbf{w}_h\, \mathrm{d}S + \int_{\partial\Omega_{\mathrm{N}}} (-p_{\mathrm{e}}\mathbf{n}_{\mathrm{b}}) \cdot \mathbf{w}_h\, \mathrm{d}S \\[2ex] + \displaystyle\int_{\partial\Omega_{\mathrm{S}}} \alpha[(\mathbf{v}_h\cdot\mathbf{n})]\mathbf{n} \cdot \mathbf{w}_h\, \mathrm{d}S - \int_{\partial\Omega_{\mathrm{S}}} \beta(\mathbf{v}_h - [(\mathbf{v}_h\cdot\mathbf{n})]\mathbf{n}) \cdot \mathbf{w}_h\, \mathrm{d}S \\[2ex] \displaystyle\int_{\Omega} q_h\, \nabla \cdot \mathbf{v}_h\, \mathrm{d}V + \int_{\Omega} \tau_h(\nabla p_h - \rho\mathbf{g}) \cdot \nabla q_h\, \mathrm{d}V = 0 \end{cases} \tag{10}$$

for all $(\mathbf{w_h}, q_h) \in (W_0)_h \times Q_h$, where $(W_0)_h$ is the finite dimensional subspace of W_0. The stabilization parameter τ_K is defined as:

$$\tau_K = \frac{h_k^2}{c_1 \eta_K}$$

with c_1 an algorithmic constant and h_K the size of the element. It was established that the numerical approximation is more precise when c_1 is larger, given that the system is stabilized, since the larger c_1 is, the smaller diffusion is added to stabilize the system. However, it is difficult to give a common value of c_1. And we note that the value of c_1 varies for different applications in the literature, for example $c_1 = 2$, 4 or 40 have been taken in [15,27,38,17].

3.2. Surface tension term computation

Since the interface is not explicitly represented on the mesh within a Eulerian context, the implementation of surface tension force (Eq. (9)):

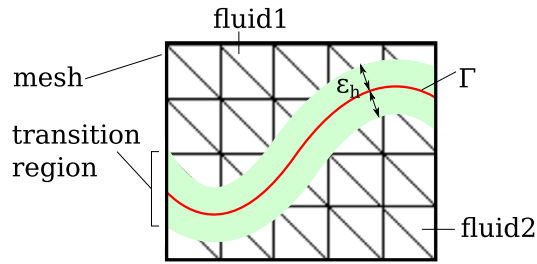$$\int_{\Gamma} \gamma\kappa\mathbf{n} \cdot \mathbf{w}\, \mathrm{d}S \tag{11}$$

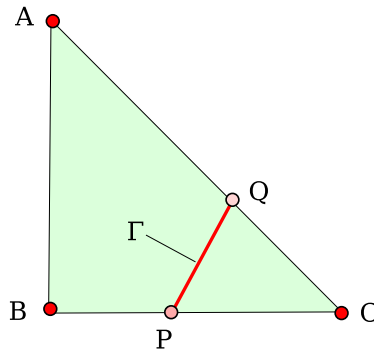**Fig. 7.** Continuum Surface Force (CSF) method.

Fig. 8. Surface Local Reconstruction (SLR) method [17].

is not straightforward. Two surface integral methods are thus studied: the Continuum Surface Force (CSF) method [18], where the surface integral is approximated by a volume integral, and the Surface Local Reconstruction (SLR) method [39,15, 17,40], where the surface tension term is explicitly computed over a locally reconstructed interface.

The CSF method is widely used in literature [18,11,28,41]. It consists in approximating the surface integral by the volume integral of the transition region as shown in Fig. 7, and can be expressed as:

$$\int_{\Gamma} \gamma \kappa \mathbf{n} \cdot \mathbf{w} \, dS = \int_{\Omega} \delta(\varphi) \gamma \kappa \mathbf{n} \cdot \mathbf{w} \, dV \tag{12}$$

The discretization of $\delta(\varphi)$ is given by:

$$\delta_h(\varphi) = \begin{cases} 0, \text{ if } |\varphi| > \epsilon_h \\ \frac{1}{2\epsilon_h}\left(1 + \cos\left(\frac{\pi\varphi}{\epsilon_h}\right)\right), \text{ if } |\varphi| \leq \epsilon_h \end{cases} \tag{13}$$

We note here that the parameter ϵ_h has to be changed with respect to the mesh size. The numerical results are strongly influenced by this parameter. In this article, the value of $0.75 h_K$ is adopted for ϵ_h, with h_K the size of the element.

The SLR method consists in reconstructing locally the interface by the iso-surface of the Level Set function $\Gamma = \{x | \varphi(x) = 0\}$, when an element is cut by the latter. The interface is thus approximated by a segment in 2D cases, or a plane in 3D cases. Then the surface integral can be calculated directly at the interface by Gaussian integration. Fig. 8 shows one of the interface–element intersection cases in 2D. In this case, the surface tension term is integrated directly on the reconstructed interface: segment PQ, more details can be found in [17].

The curvature, defined as $\kappa = \nabla \cdot \mathbf{n}$, cannot be computed directly, because the Level Set function is piecewise linear, and the normals are piecewise constant. The first method for the curvature computation consists in re-projecting the normal vectors on each nodes and then computing the divergence of the P1 normal field. However, the interpolation of normal in this method can be a source of numerical errors. Thus, an alternative tensorial method (Eq. (18)) [19,17] has been implemented for the weak form. Since the mean curvature can be defined as the surface divergence of the unit normal $\nabla_s \cdot \mathbf{n}$, it equals to the trace of the surface gradient operator:

$$\kappa = \nabla_s \cdot \mathbf{n} = [\mathbb{1} - \mathbf{n} \otimes \mathbf{n}] : \nabla \mathbf{n} \tag{14}$$

then the surface tension term can be written as:

Algorithm 1 Static angle computation algorithm.

1: **while** $\theta \neq \alpha$ **do**
2: compute the normal vector field ($\mathbf{n}_\Gamma = \frac{\nabla \varphi}{\|\nabla \varphi\|}$), φ function Level Set
3: compute the normal vector of fiber outer boundary ($\mathbf{n}_S$)
4: compute the normal vector $\mathbf{n}_\theta = R_\theta \cdot \mathbf{n}_S$
5: replace $\mathbf{n}_\Gamma$ at the fluid/solid interface by $\mathbf{n}_\theta$
6: compute curvature field (κ)
7: compute the surface tension force using Eq. (11)
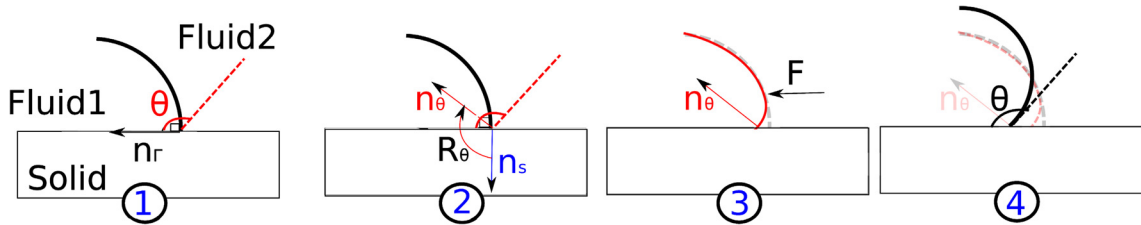8: solve Stokes' equations
9: move the interface

Fig. 9. Static angle computation sketch.

$$\int_\Gamma \gamma \, \kappa \, \mathbf{n} \cdot \mathbf{w} \, \mathrm{d}S$$

$$= \int_\Gamma \gamma \, \nabla_s \cdot \mathbf{n} \, (\mathbf{n} \cdot \mathbf{w}) \, \mathrm{d}S$$

$$= \int_\Gamma \gamma \, ([\mathbb{1} - \mathbf{n} \otimes \mathbf{n}] : \nabla \mathbf{n}) \, (\mathbf{n} \cdot \mathbf{w}) \, \mathrm{d}S$$

$$= \int_\Gamma \gamma [\mathbb{1} - \mathbf{n} \otimes \mathbf{n}] : \nabla (\mathbf{n} \otimes \mathbf{n} \cdot \mathbf{w}) \, \mathrm{d}S \tag{15}$$

Moreover, since $\mathbb{1} - \mathbf{n} \otimes \mathbf{n}$ is the operator of projection onto the tangent space of Γ, the vector $(\mathbb{1} - \mathbf{n} \otimes \mathbf{n}) \cdot \mathbf{w}$ is tangent to Γ. Thus when the surface Γ is closed, the following relation holds:

$$\int_\Gamma \gamma \, \nabla_s \cdot ([\mathbb{1} - \mathbf{n} \otimes \mathbf{n}] \cdot \mathbf{w}) \, \mathrm{d}S = 0 \tag{16}$$

then the right-hand term in Eq. (15) can be written as:

$$\int_\Gamma \gamma [\mathbb{1} - \mathbf{n} \otimes \mathbf{n}] : \nabla (\mathbf{n} \otimes \mathbf{n} \cdot \mathbf{w}) \, \mathrm{d}S \overset{\Gamma \text{ closed}}{=} \int_\Gamma \gamma [\mathbb{1} - \mathbf{n} \otimes \mathbf{n}] : \nabla \mathbf{w} \, \mathrm{d}S \tag{17}$$

Therefore, the surface tension term can be computed using the following relation:

$$\int_\Gamma \gamma \kappa \mathbf{n} \cdot \mathbf{w} \, \mathrm{d}S = \int_\Gamma \gamma [\mathbb{1} - \mathbf{n} \otimes \mathbf{n}] : \nabla \mathbf{w} \, \mathrm{d}S \tag{18}$$

We note that the relation (18), called the tensorial method, is valid only when the surface Γ is closed. Thereafter, the tensorial method is only applied for flow dynamics cases, the first method is considered for contact line problems.

3.3. Static angle computation

Here is presented an iterative method to take into account the static angle. This method is proposed in [42] for an ALE computation, and used in [43] with a P1+/P1 stabilization method within an Eulerian representation. The computation algorithm is shown in **Algorithm 1**, it aims at prescribing the contact angle by normal $\mathbf{n}_\theta$ (Fig. 9). We replace firstly the normal vector $\mathbf{n}_\Gamma$, computed from the gradient of the Level Set function, by $\mathbf{n}_\theta$ at the fluid/solid interface (Fig. 9 ②). $\mathbf{n}_\theta$ is calculated from the desired angle θ and from the normal vector $\mathbf{n}_S$ of the solid surface. In fact, $\mathbf{n}_\theta = R_\theta \cdot \mathbf{n}_S$, where R_θ is the rotation matrix which perform a rotation of n_S through an angle θ. This modification introduces a local modification of the curvature. Since the surface tension has effects to smooth the curvature, a force is generated naturally to move the interface till it matches the desired angle (Fig. 9 ③, ④).
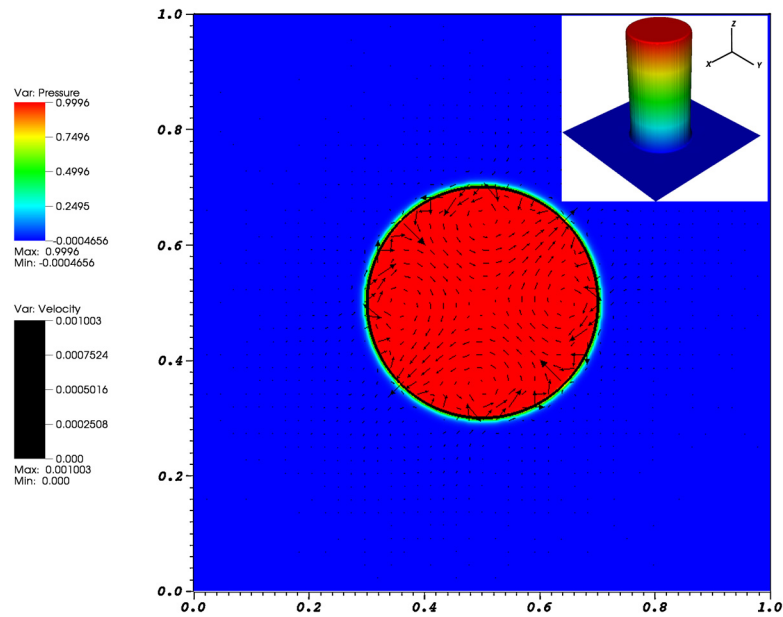
Fig. 10. Pressure and velocity fields for a static bubble under surface tension effect. $\gamma = 0.2$ N $\cdot$ m^{-1}, viscosity of the fluid inner the bubble: 0.1 Pa $\cdot$ s, and the outer fluid 0.001 Pa $\cdot$ s.
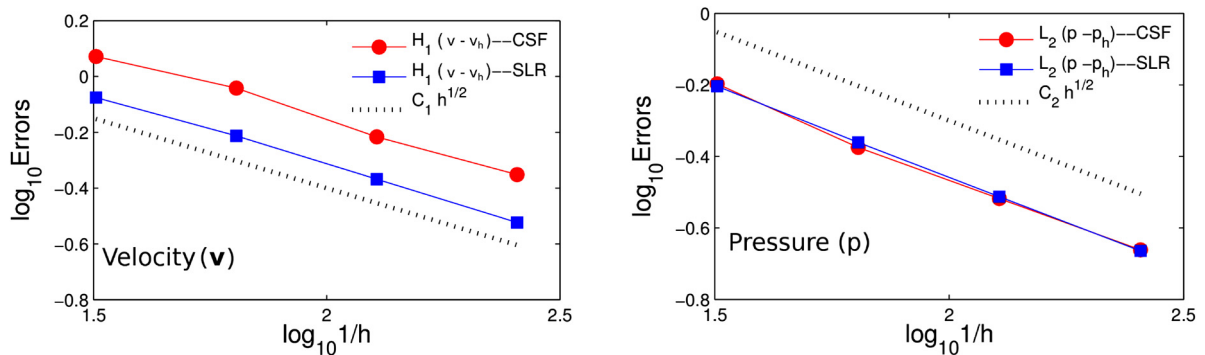

Fig. 11. Convergence curves of velocity and pressure for the static bubble case.

4. Results and discussion

In this section, capillary-driven flow test cases are first investigated. Convergence studies have been carried out on a 2D static case. Then, fluid dynamic cases are simulated and compared to analytical solutions. The fluid volume conservation has been verified. Thereafter, wetting phenomena are illustrated on test case of static droplet on a plane wall considering different contact angles.

4.1. Static bubble

We consider here a 2D test case to check the convergence and the performance of the different methods developed so far. The test consists in computing the equilibrium of a static bubble placed inside another fluid. The bubble interface is a circle of radius 0.2 m, the fluid domain is a (1 m $\times$ 1 m) square. The surface tension is considered at the interface, γ is 0.2 N $\cdot$ m^{-1}. The viscosity is 0.1 Pa $\cdot$ s for the fluid inside the bubble and is 0.001 Pa $\cdot$ s for the fluid surrounding. The analytical solution to this problem is a zero velocity field and a discontinuous pressure field due to the surface tension effect. The pressure jump at interface is $\Delta p = \gamma \kappa = 1$ Pa according to the Laplace law. Due to numerical approximations, spurious velocities could be observed at the vicinity of the interface (Fig. 10). Following various authors [17,11,15], viscosity discontinuities and γ/κ ratio are the key parameters to control the stability of this kind of simulations: the larger these parameters are, the more pronounced parasitic currents are. Here we compare the two methods for the surface integration: CSF and SLR. The errors in the L^2-norm for the pressure and H^1-norm for the velocity show a convergence rate of 1/2 for both methods (Fig. 11), which is the expected value, since the discontinuous pressure field is approximated by continuous P1 space across the interface [14]. The convergence curves are obtained using four regular triangle meshes, with respectively
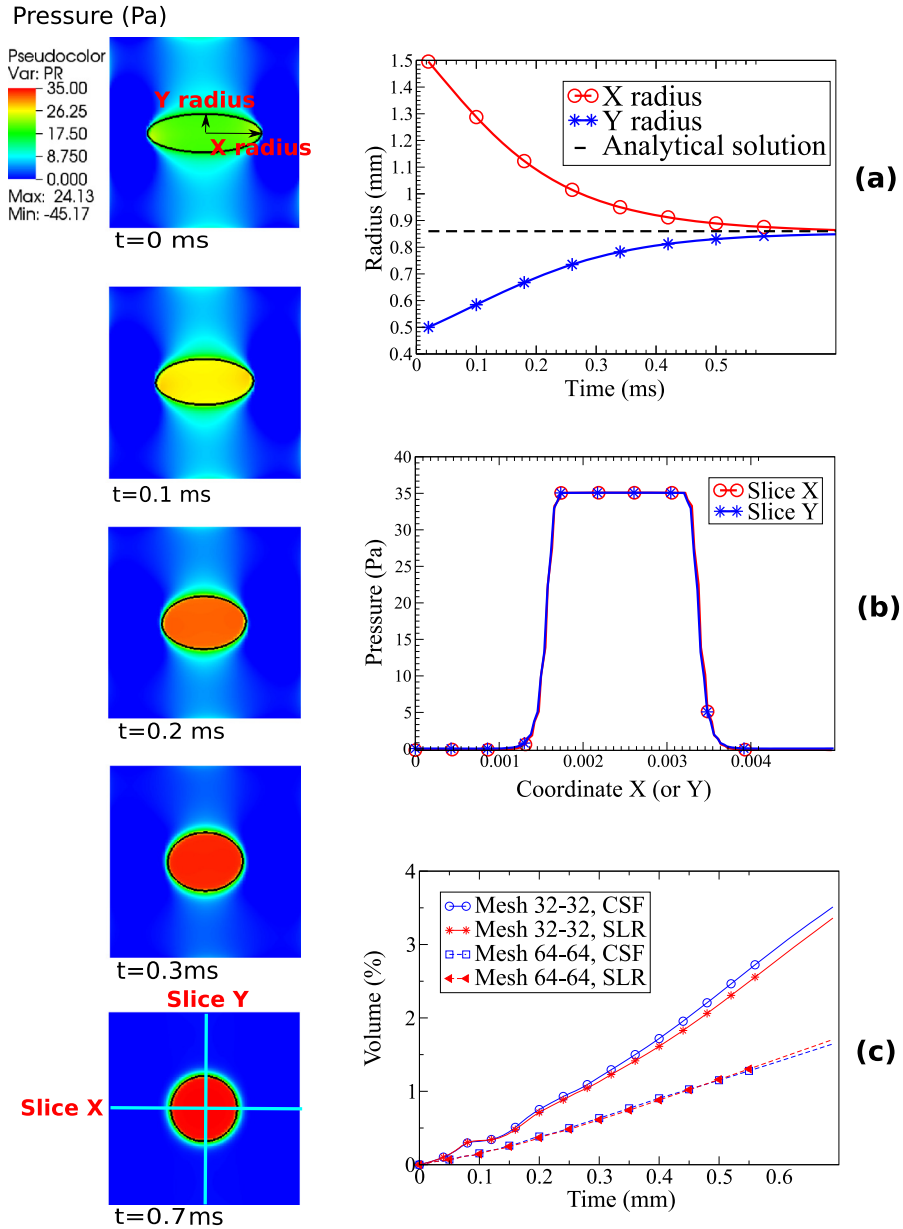
Fig. 12. An ellipse shape bubble evolution under the surface tension effect, $\gamma = 0.03$ N · m^{-1}, viscosity of fluid inner the ellipse: 0.3 mPa · s, viscosity of surrounding fluid: 30 mPa · s. (a) The radius evolution of the X- and Y-axes of the ellipse; (b) pressure of two slices of fluid domain at $t = 0.7$ ms; (c) volume loss for different calculations.

32, 64, 128 and 256 nodes on each domain side. Both methods have nearly the same precisions for pressure fields, the SLR method is more precise than the CSF one for the velocity approximation.

4.2. Ellipse evolution

The evolution of an ellipse under the surface tension effect is simulated. As shown in Fig. 12, the ellipse turns to a circle under the surface tension force effect. We consider here an ellipse of radius 0.5 mm × 1.5 mm, enclosed in a squared domain of 5 mm × 5 mm. The surface tension coefficient is 0.03 N · m^{-1}. The viscosity is 0.0003 Pa · s for the fluid inner the ellipse and 0.03 Pa · s for the surrounding fluid. The numerical values of the viscosities and the surface tension coefficient are realistic values for thermoset resin such as RTM6 at 120 °C and air [30]. Since the volume of the ellipse is conserved, the analytic solution is that the bubble becomes a circle of radius $R = 0.86$ mm and the pressure jump at the interface is $\Delta p = \gamma \kappa = 34.8$ Pa, with $\kappa = \dfrac{1}{R}$ according to the Laplace law. The numerical simulations have been carried out using both
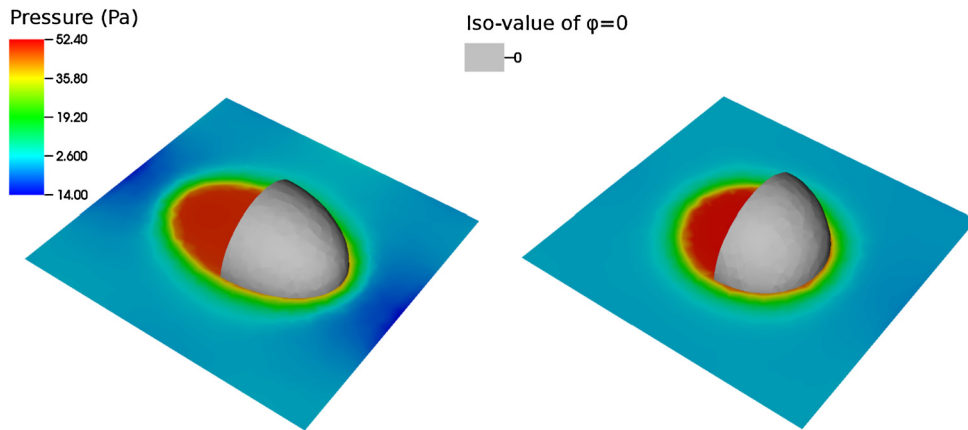
Fig. 13. An ellipsoid evolution (3D) under the surface tension effect, $\gamma = 0.03$ N·m^{-1}, viscosity of both fluids: 30 mPa·s and 0.3 mPa·s. The plan is a slice of the pressure field.
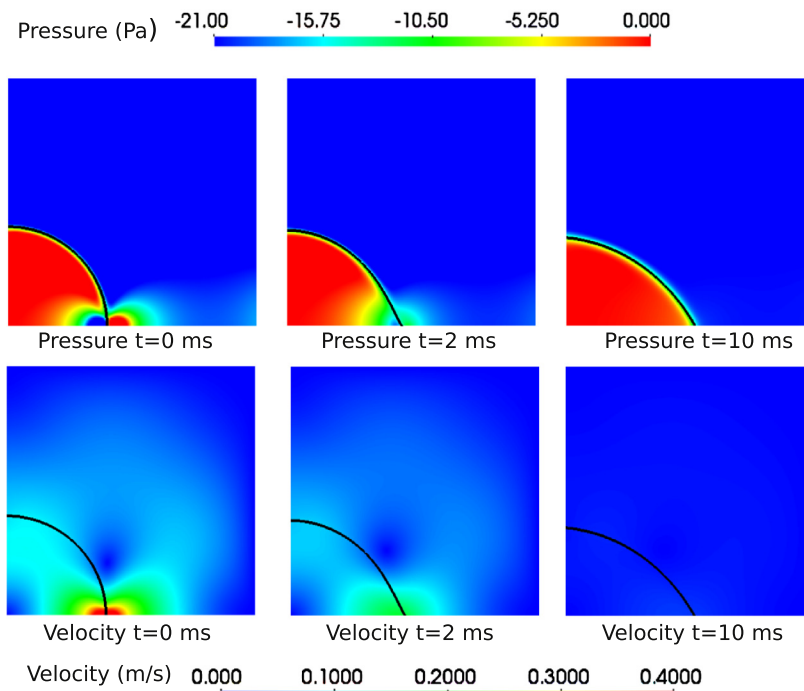
Fig. 14. Discontinuous pressure fields (2D) for the simulation of a droplet on a substrate with a contact angle of 60°, $\gamma = 0.07$ N·m^{-1}, viscosity of both fluids: 0.03 Pa·s, $\Delta t = 0.2$ ms.

surface tension integration methods (CSF and SLR), combined with two regular triangle meshes with respectively 32 nodes or 64 nodes on each domain side, denoted mesh 32–32 and mesh 64–64. The ASGS stabilization parameter c_1 is set at 100. The CSF approximation gives results very similar to the SLR method. The results obtained with the SLR method and mesh 64–64 are presented in Fig. 12: the radius of the ellipse converges to a value of 0.85 mm (Fig. 12), the pressure jump is 35 Pa at the interface (Fig. 12). These results are in very good agreement with the analytical solutions in terms of pressure jump (error < 1%) and final radius of the circle shape (error < 1.5%). Fig. 12 shows that the SLR method conserves slightly better the bubble volume than the CSF method. However, the bubble volume is well conserved for both methods during this process (less than 4% difference from the beginning to the end of calculation). A 3D simulation is also performed (Fig. 13). We consider here an ellipse of 1 mm × 1 mm × 1.5 mm enclosed in a cube of 5 mm × 5 mm × 5 mm. The fluid parameters are the same as that of the 2D case. The analytical solution is that the ellipsoid turns to a sphere of radius 1.1447 mm, with a pressure jump of 52.4 Pa at the interface. An unstructured mesh with tetrahedron elements, which has nearly 40 elements on every edge and 240,831 elements in total is considered. The value of $c_1 = 100$ is adopted. The numerical pressure jump is 54.3 Pa for the CSF method and 55.8 Pa for the SLR method, which is of respectively 3.6% and 6.4% difference compared
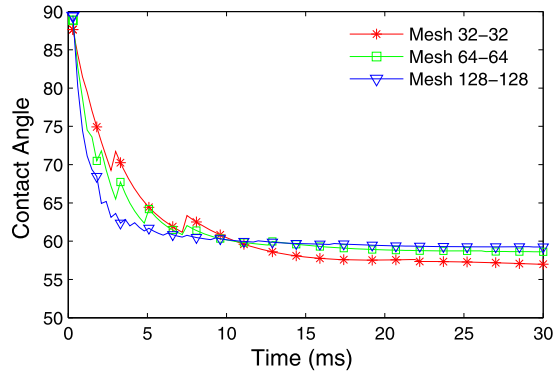
Fig. 15. Contact angle change *vs.* time of the droplet on a substrate test case (2D, Fig. 14) for 32×32, 64×64, 128×128 regular meshes, $\Delta t = 0.2$ ms.

Table 1
Analytical values of H, R and Δp for different contact angles of droplet on a substrate test case (3D).

θ	H (height)	R (radius)	Δp (pressure jump)
60°	1.47 mm	2.94 mm	20.35 Pa
75°	1.73 mm	2.33 mm	25.75 Pa
120°	2.52 mm	1.68 mm	35.72 Pa
150°	2.97 mm	1.59 mm	37.74 Pa
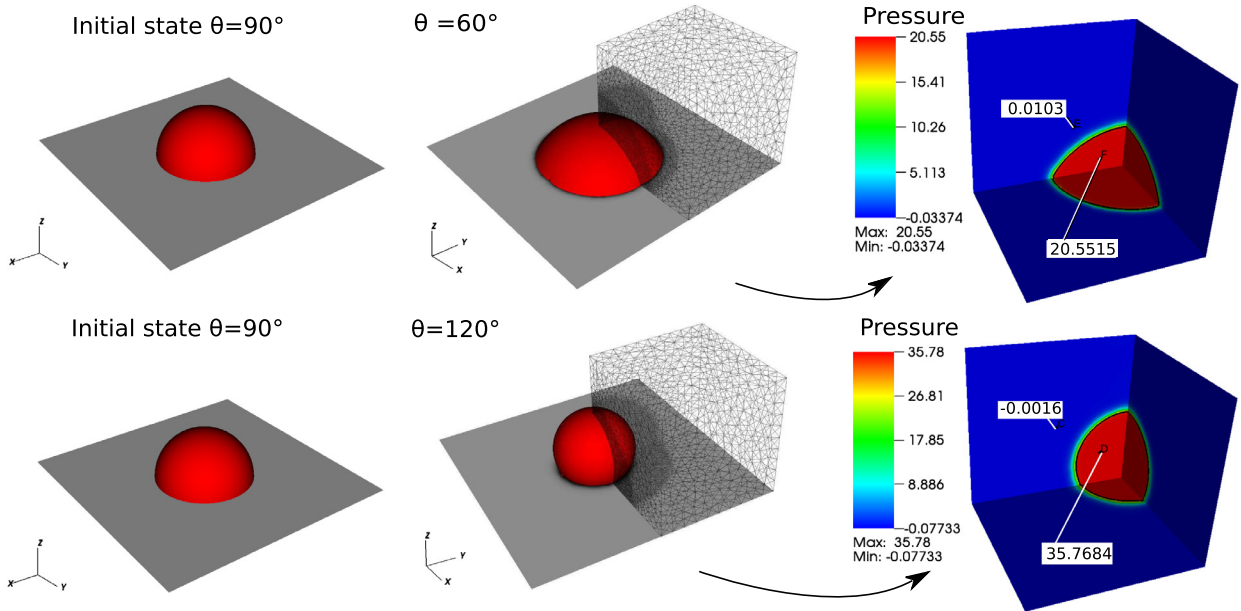
Fig. 16. Drop evolution with a contact angle of 60° (top) and 120° (bottom) over a plane substrate, $\gamma = 0.03$ N · m^{-1}, viscosity of fluids: 30 mPa · s (drop) and 0.3 mPa · s (surrounding fluid).

to the analytical solution. The initial and final state of the ellipsoid shape for the CSF method are shown in Fig. 13, only a quarter of the iso-value surface is drawn for clarity.

4.3. Static drop on a plane wall

The evolution of a liquid drop, initially a quarter of sphere, in contact with a plane wall is modelled. Starting from an initial contact angle of 90°, the liquid flow is computed until the drop shape stabilizes. The liquid is submitted to surface tension, and the wetting boundary conditions (section 2.3) are applied to the fluids/solid interface. In this case, we are interested in the equilibrium of the droplet; $\beta = 0$ is adopted here to avoid the contact line dissipation [27], the contact with the wall is thus frictionless.
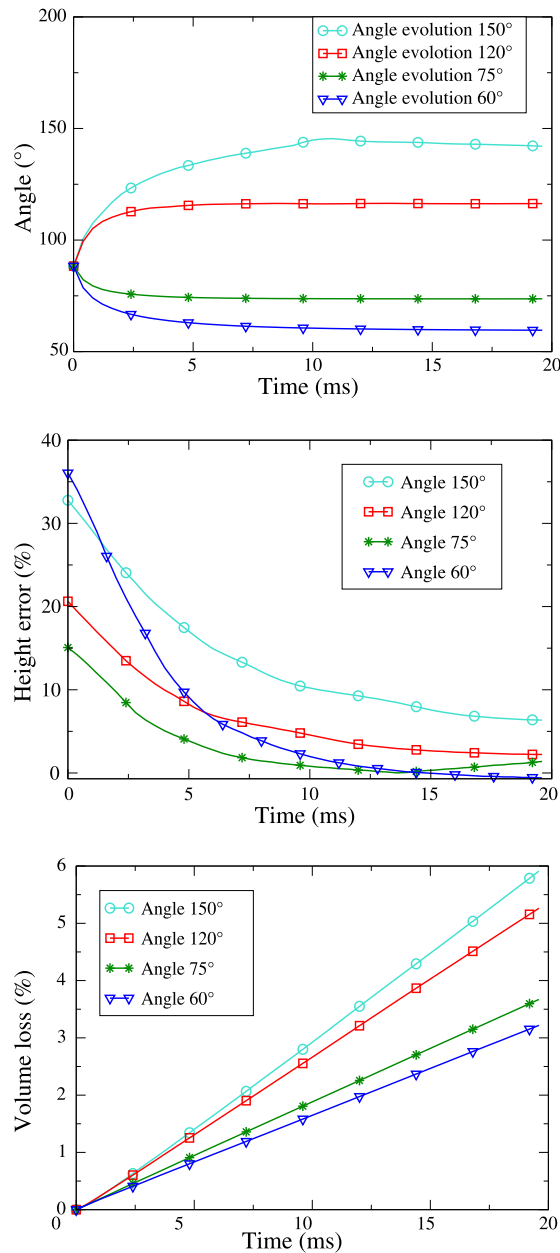
Fig. 17. Contact angles (average over the contact line), height evolution and volume loss of droplet on a substrate test case (3D) with a contact angle of 60°, 75°, 120° and 150°, $\Delta t = 0.4$ ms.

A 2D case is first verified with a target contact angle of 60°. It is applied only to the bottom of the domain and a symmetry condition ($\mathbf{v} \cdot \mathbf{n}_s = 0$, $\mathbf{n}_s$ normal of outer boundary) is applied to the left boundary of the domain (Fig. 14). The square domain is of 5 mm × 5 mm, the radius of the droplet is 2 mm. The dynamic viscosity of both fluids is $\eta = 0.03$ Pa · s. The surface tension coefficient is $\gamma = 0.07$ N · m^{-1}. The simulation is performed on three regular triangle meshes, with respectively 32, 64 and 128 nodes on each domain boundary, and denoted mesh 32–32, mesh 64–64 and mesh 128–128. The numerical results of mesh 128–128 are presented in Fig. 14. One can see that the fluid domain configuration converges towards a stable shape, which is reached after about 50 Stokes' equation-solving increments (10 ms approximately, with a time step of $\Delta t = 0.2$ ms). The contact angle's evolution according to different mesh element size is plotted in Fig. 15.

Four contact angles, 60°, 75°, 120° and 150° have been considered for the 3D simulations. The dynamic viscosity of the inner fluid is $\eta = 0.03$ Pa · s and $\eta = 0.0003$ Pa · s for the surrounding fluid. The surface tension coefficient is $\gamma = 0.03$ N · m^{-1}. The height H and the radius R of the equilibrium drop, which should be a truncated sphere shape, can be calculated thanks to the volume conservation property. The pressure jump at interface can also be calculated as $\Delta p = \gamma \kappa$,

with $\kappa = \dfrac{2}{R}$ according to the Laplace's law. The analytical values of H, R and Δp for different contact angles are shown in Table 1.

Here, only a quarter domain is computed, as shown in Fig. 16. The other part is represented thanks to the symmetry condition. In fact, the symmetry condition reads: $\mathbf{v} \cdot \mathbf{n} = 0$, θ (contact angle) $= 90°$ applied to the two lateral surfaces of the computation domain for symmetry purpose. Since the iso-surface is prescribed by a plane in an element, we refined the mesh at the vicinity of the drop plane interface so as to have a correct geometry representation. The element size varies from 0.08 mm to 0.5 mm regarding the distance to the interface. The mesh is made up of 24,458 nodes and 138,688 tetrahedral linear elements. The initial and final drop shapes for the contact angle of 60° and 120° are presented in Fig. 16, the pressure jump at the interface is in good agreement with the analytical solution (error < 1%). The contact angle evolutions are shown in Fig. 17. This value is the average of contact angles along the contact line between the drop and the plane wall. The mean value of the contact angle converges towards the prescribed value in about 13 Stokes' equation-solving increments (5 ms approximately with a time step of $\Delta t = 0.4$ ms, Fig. 17). The drops height agrees well with the analytical results, the numerical errors can be observed less than 5% for the stable state. The volume of the drop is also well conserved during this simulation, less than 5% volume loss for both test cases. Moreover, the numerical errors increase with the value of the prescribed contact angle, since for the same drop volume, when the contact angle increases, the associated radius decreases and the interface curvature increases, and so does the numerical errors associated with the surface tension term.

5. Conclusions

The aim of this work was to study some problems involving capillarity and wetting, as those typically met in the manufacturing processes by resin infusion, within a framework of finite element methods. A local fluid–solid contact model has been established to take into account those effects. This model is based on a Eulerian description of two immiscible fluid domains with boundary conditions describing wetting phenomena at fluid/fiber interfaces. The fluid interface is described by the Level Set method, on which capillary force are considered. One of the bottle necks of this method is the spurious velocity related to the singular surface tension force at the interface. Two surface tension computation methods have thus been developed and compared on different test cases. Numerical methods allowing one to take into account the static contact angle and the contact line motion have been implemented and verified thereafter. Several outlooks can be drawn from this work. First, even if the numerical precision of capillary interface simulation is satisfying in 2D, more effort is still necessary for 3D simulations. Second, the dynamic of the contact line motion requires some consideration and will be investigated in future works.

References

[1] P. Celle, S. Drapier, J.-M. Bergheau, Numerical modelling of liquid infusion into fibrous media undergoing compaction, Eur. J. Mech. A-Solids 27 (4) (2008) 647–661.
[2] L. Abouorm, N. Moulin, J. Bruchon, S. Drapier, Monolithic approach of Stokes–Darcy coupling for LCM process modelling, Key Eng. Mater. 554 (2013) 447–455.
[3] L. Abouorm, M. Blais, N. Moulin, J. Bruchon, S. Drapier, A robust monolithic approach for resin infusion based process modelling, in: Key Engineering Materials, vol. 611, 2014, pp. 306–315.
[4] A. Dereims, S. Drapier, J.-M. Bergheau, P. de Luca, 3D robust iterative coupling of Stokes, Darcy and solid mechanics for low permeability media undergoing finite strains, Finite Elem. Anal. Des. 94 (2015) 1–15.
[5] F.H. Harlow, J.E. Welch, et al., Numerical calculation of time-dependent viscous incompressible flow of fluid with free surface, Phys. Fluids 8 (12) (1965) 2182.
[6] S. Osher, J.A. Sethian, Fronts propagating with curvature-dependent speed: algorithms based on Hamilton–Jacobi formulations, J. Comput. Phys. 79 (1) (1988) 12–49.
[7] J.A. Sethian, Level Set Methods and Fast Marching Methods: Evolving Interfaces in Computational Geometry Fluid Mechanics, Computer Vision, and Materials Science, vol. 3, Cambridge University Press, 1999.
[8] C.W. Hirt, B.D. Nichols, Volume of fluid (VOF) method for the dynamics of free boundaries, J. Comput. Phys. 39 (1) (1981) 201–225.
[9] G. Tryggvason, B. Bunner, A. Esmaeeli, D. Juric, N. Al-Rawahi, W. Tauber, J. Han, S. Nas, Y.-J. Jan, A front-tracking method for the computations of multiphase flow, J. Comput. Phys. 169 (2) (2001) 708–759.
[10] E. Maitre, Review of numerical methods for free interfaces, in: Ecole Thématique "Modèles de champ de phase pour l'évolution de structures complexes", Les Houches, 2006.
[11] A. Smolianski, Numerical modeling of two-fluid interfacial flows, PhD thesis, University of Jyväskylä, 2001.
[12] M. van Sint Annaland, N. Deen, J. Kuipers, Numerical simulation of gas bubbles behaviour using a three-dimensional volume of fluid method, Chem. Eng. Sci. 60 (11) (2005) 2999–3011.
[13] M. Sussman, M. Ohta, High-order techniques for calculating surface tension forces, in: Free Boundary Problems, Springer, 2007, pp. 425–434.
[14] S. Groß, A. Reusken, An extended pressure finite element space for two-phase incompressible flows with surface tension, J. Comput. Phys. 224 (1) (2007) 40–58.
[15] R.F. Ausas, F.S. Sousa, G.C. Buscaglia, An improved finite element space for discontinuous pressures, Comput. Methods Appl. Mech. Eng. 199 (17) (2010) 1019–1031.
[16] S. Ganesan, G. Matthies, L. Tobiska, On spurious velocities in incompressible flow problems with interfaces, Comput. Methods Appl. Mech. Eng. 196 (7) (2007) 1193–1202.
[17] D. Pino Muñoz, J. Bruchon, S. Drapier, F. Valdivieso, A finite element-based level set method for fluid–elastic solid interaction with surface tension, Int. J. Numer. Methods Eng. 93 (9) (2013) 919–941.
[18] J. Brackbill, D.B. Kothe, C. Zemach, A continuum method for modeling surface tension, J. Comput. Phys. 100 (2) (1992) 335–354.
[19] Y. Demay, A. Béliveau, A. Fortin, A numerical method for the deformation of two-dimensional drops with surface tension, Int. J. Comput. Fluid Dyn. 10 (1998) 225–240.

[20] P.-G. De Gennes, Wetting: statics and dynamics, Rev. Mod. Phys. 57 (3) (1985) 827.

[21] D. Bonn, J. Eggers, J. Indekeu, J. Meunier, E. Rolley, Wetting and spreading, Rev. Mod. Phys. 81 (2) (2009) 739.

[22] T. Qian, X.-P. Wang, P. Sheng, Molecular scale contact line hydrodynamics of immiscible flows, Phys. Rev. E 68 (1) (2003) 016306.

[23] W. Ren, E. Weinan, Boundary conditions for the moving contact line problem, Phys. Fluids 19 (2) (2007) 022101.

[24] H. Kusumaatmaja, J.M. Yeomans, Lattice Boltzmann simulations of wetting and drop dynamics, in: Simulating Complex Systems by Cellular Automata, Springer, 2010, pp. 241–274.

[25] Y. Sui, H. Ding, P.D. Spelt, Numerical simulations of flows with moving contact lines, Annu. Rev. Fluid Mech. 46 (2014) 97–119.

[26] Y. Yamamoto, K. Tokieda, T. Wakimoto, T. Ito, K. Katoh, Modeling of the dynamic wetting behavior in a capillary tube considering the macroscopic–microscopic contact angle relation and generalized Navier boundary condition, Int. J. Multiph. Flow 59 (2014) 106–112.

[27] G.C. Buscaglia, R.F. Ausas, Variational formulations for surface tension, capillarity and wetting, Comput. Methods Appl. Mech. Eng. 200 (45) (2011) 3011–3025.

[28] J. Sprittles, Y. Shikhmurzaev, Finite element framework for describing dynamic wetting phenomena, Int. J. Numer. Methods Fluids 68 (10) (2012) 1257–1298.

[29] J.-F. Gerbeau, T. Lelievre, Generalized Navier boundary condition and geometric conservation law for surface tension, Comput. Methods Appl. Mech. Eng. 198 (5) (2009) 644–656.

[30] M. Pucci, P.-J. Liotier, S. Drapier, Capillary effects on flax fibres-modification and characterisation of the wetting dynamics, Compos. Part A Appl. Sci. Manuf. 77 (2015) 257–265, http://dx.doi.org/10.1016/j.compositesa.2015.03.010.

[31] M. Sussman, P. Smereka, S. Osher, A level set approach for computing solutions to incompressible two-phase flow, J. Comput. Phys. 114 (1) (1994) 146–159.

[32] A.N. Brooks, T.J. Hughes, Streamline upwind/Petrov–Galerkin formulations for convection dominated flows with particular emphasis on the incompressible Navier–Stokes equations, Comput. Methods Appl. Mech. Eng. 32 (1) (1982) 199–259.

[33] C. Navier, Mémoire sur les lois du mouvement des fluides, Mém. Acad. Sci. Inst. Fr. 6 (1823) 389–440.

[34] E. Dussan, On the spreading of liquids on solid surfaces: static and dynamic contact lines, Annu. Rev. Fluid Mech. 11 (1) (1979) 371–400.

[35] J.-B. Dupont, D. Legendre, Numerical simulation of static and sliding drop with contact angle hysteresis, J. Comput. Phys. 229 (7) (2010) 2453–2478.

[36] S. Badia, R. Codina, Unified stabilized finite element formulations for the Stokes and the Darcy problems, SIAM J. Numer. Anal. 47 (3) (2009) 1971–2000.

[37] L. Abouorm, R. Troian, S. Drapier, J. Bruchon, N. Moulin, Stokes–Darcy coupling in severe regimes using multiscale stabilisation for mixed finite elements: monolithic approach versus decoupled approach, Eur. J. Comput. Mech. 23 (3–4) (2014) 113–137.

[38] H. Coppola-Owen, R. Codina, A free surface finite element model for low Froude number mould filling problems on fixed meshes, Int. J. Numer. Methods Fluids 66 (7) (2011) 833–851.

[39] E. Aulisa, S. Manservisi, R. Scardovelli, S. Zaleski, Interface reconstruction with least-squares fit and split advection in three-dimensional Cartesian geometry, J. Comput. Phys. 225 (2) (2007) 2301–2319.

[40] D. Pino-Muñoz, J. Bruchon, S. Drapier, F. Valdivieso, Sintering at particle scale: an Eulerian computing framework to deal with strong topological and material discontinuities, Arch. Comput. Methods Eng. 21 (2) (2014) 141–187.

[41] S. Zahedi, M. Kronbichler, G. Kreiss, Spurious currents in finite element based level set methods for two-phase flow, Int. J. Numer. Methods Fluids 69 (9) (2012) 1433–1456.

[42] M. Bellet, Implementation of surface tension with wall adhesion effects in a three-dimensional finite element model for fluid flow, Commun. Numer. Methods Eng. 17 (8) (2001) 563–579.

[43] G. Puaux, Simulation numérique des écoulements aux échelles microscopique et mésoscopique dans le procédé RTM, PhD thesis, École nationale supérieure des mines de Paris, 2011.